NONLINEAR VIBRATION ANALYSIS OF MICROSCALE FUNCTIONALLY GRADED TIMOSHENKO BEAMS USING THE MOST GENERAL FORM OF STRAIN GRADIENT ELASTICITY

R. Ansari * **M. Faghih Shojaei** **V. Mohammadi** **R. Gholami** **H. Rouhi**

Department of Mechanical Engineering
University of Guilan
Rasht, Iran

ABSTRACT

Based on the Timoshenko beam model, the nonlinear vibration of microbeams made of functionally graded (FG) materials is investigated under different boundary conditions. To consider small scale effects, the model is developed based on the most general form of strain gradient elasticity. The nonlinear governing equations and boundary conditions are derived via Hamilton's principle and then discretized using the generalized differential quadrature technique. A pseudo-Galerkin approach is used to reduce the set of discretized governing equations into a time-varying set of ordinary differential equations of Duffing-type. The harmonic balance method in conjunction with the Newton-Raphson method is also applied so as to solve the problem in time domain. The effects of boundary conditions, length scale parameters, material gradient index and geometrical parameters are studied. It is found that the importance of the small length scale is affected by the type of boundary conditions and vibration mode. Also, it is revealed that the classical theory tends to underestimate the vibration amplitude and linear frequency of FG microbeams.

Keywords: Timoshenko microbeam, Functionally graded material, Nonlinear vibration, Most general form of strain gradient elasticity.

1. INTRODUCTION

Microbeams and microplates are important structural components in micro-engineering applications, such as in micromechanical systems (MEMS) and atomic force microscopes (AFMs). Based on the classical continuum theory, several researchers studied the mechanical behavior of microbeams [1-11] and microplates [12-16].

It is experimentally observed that the mechanical behavior of micro-structures is size-dependent [17-19]. Since the classical continuum theory cannot predict the small scale effects, size-dependent continuum theories such as strain gradient theory (SGT) [20,21] and couple stress theory (CST) [22,23] have been proposed to accommodate the size dependence of micro-structures. In the CST, two material length scale parameters (in addition to two classical material constants) are used in order to capture the size effects. Whereas, in the modified couple stress theory (MCST) [24], the constitutive equations contain only one additional material length scale parameter. In comparison with the CST, the SGT includes some higher-order stresses in addition to classical and couple stresses. In the modified strain gradient theory (MSGT) [25], three material length scale parameters associated with the dilatation gradient tensor, deviatoric gradient tensor and symmetric rotation gradient tensor are considered.

From the published papers, it is revealed that many studies have been conducted on the mechanical behavior of micr-ostructures based on the size-dependent continuum theories. Asghari *et al*. [26] developed a size-dependent Euler-Bernoulli beam model based on the MCST in order to study the static and vibration characteristics of FG microbeams. Ke *et al*. [27] investigated the effect of temperature change on the free vibration and buckling of Timoshenko microbeams on the basis of MCST. Ke and Wang [28] studied the dynamic stability of FG Timoshenko microbeams using the MCST. Ansari and his co-workers [29] developed a SGT Timoshenko beam model to analyze the free vibration of FG microbeams. Ke *et al*. [30] used the MCST in conjunction with the Mindlin plate theory so as to address the bending, buckling and free vibration of FG annular microplates. Ansari *et al*. [31] studied the nonlinear free vibrations of FG Timoshenko microbeams using the SGT. The free vibration analysis of Mindlin microplates was presented by Ke *et al*. [32] based upon the MCST. Within the framework of MCST, Kahrobaiyan *et al*. [33] developed an Euler-Bernoulli beam model in order to investigate the nonlinear forced vibration of microbeams. Ahmadi and

* Corresponding author (r_ansari@guilan.ac.ir)

DOI : 10.1017/jmech.2013.65
Copyright © 2014 The Society of Theoretical and Applied Mechanics, R.O.C.
https://doi.org/10.1017/jmech.2013.65 Published online by Cambridge University Press

his associates [34] studied the buckling of rectangular flexural microplates using the MCST. Based on the SGT with the inclusion of surface energy, Rajabi and Ramezani [35] developed a nonlinear Euler-Bernoulli beam model for the vibration of microbeams. Ansari *et al*. [36] employed the SGT to study the nonlinear vibration of Timoshenko microbeams. Simsek and his co-workers [37] analyzed the static bending of FG Timoshenko microbeams based on the MCST. Sahmani and Ansari [38] analyzed the free vibration behavior of FG microplates applying a non-classical higher-order shear deformable plate model together with the SGT. Nateghi and Salamat-talab [39] presented the thermal effect on the free vibration and buckling of FG microbeams on the basis of MCST. Salamat-talab *et al*. [40] studied the bending, buckling and free vibration of FG Euler-Bernoulli microbeams via the SGT. Ansari *et al*. [41] investigated the pull-in instability of circular microplates subjected to uniform hydrostatic and non-uniform electrostatic actuations based on the MSGT. Also, it should be mentioned that surface effect is considered to be an important physical mechanism for the size-dependent mechanical responses of micro- and nano-structures. In this regard, there are several works in which the surface elasticity theory has been used to investigate the surface effect on the mechanical behavior of micro- and nano-structures [42-46].

In this paper, the nonlinear vibration of FG Timoshenko microbeams subject to different boundary conditions is studied using the most general form of strain gradient elasticity. First, Hamilton's principle along with the von Karman hypothesis is applied to derive the nonlinear governing equations and boundary conditions. The governing equations and boundary conditions are then discretized via the generalized differential quadrature (GDQ) method. A Galerkin-based scheme is applied to reduce the set of discretized governing equations into a set of Duffing-type ordinary differential equations. Using the present pseudo-Galerkin scheme, both essential and natural boundary conditions are satisfied since the linear mode shapes used in the scheme are obtained from a numerical method. Furthermore, small scale effects are incorporated into the model as the linear mode shapes are obtained based on the strain gradient elasticity theory instead of classical elasticity theory. Accordingly, by the present pseudo-Galerkin method, one can obtain the desired accuracy by a lower number of mode shapes which considerably reduces the computational cost. Finally, the harmonic balance method together with the Newton-Raphson technique is used to solve the problem in time domain. Numerical results are presented to show the effects of material gradient index, length scale parameters, boundary conditions and length-to-thickness ratio on the nonlinear vibration of FG microbeams.

2. PRELIMINARIES

According to the most general form of strain gradient elasticity [20,21], the stored strain energy in a continuum made of a linear elastic material occupying region V under infinitesimal deformations is evaluated by

$$\prod_s = \frac{1}{2}\int_v (\sigma : \varepsilon + \tau \vdots \xi)\, dV \tag{1}$$

in which σ, τ, ε and ξ are respectively stress, double stress, strain and third order strain gradient tensors. The strain tensors are written as

$$\varepsilon = \frac{1}{2}\left[\nabla u + (\nabla u)^T\right], \quad \varepsilon_{ij} = \frac{1}{2}(u_{i,j} + u_{j,i}), \tag{2a}$$

$$\xi = \nabla\varepsilon = \frac{1}{2}\nabla\left[\nabla u + (\nabla u)^T\right],$$
$$\xi_{ijk} = \xi_{ikj} = \varepsilon_{jk,i} = \frac{1}{2}(u_{j,k} + u_{k,j})_{,i}. \tag{2b}$$

where u_i shows the components of the displacement vector **u**. The stress tensors are given by

$$\sigma_{ij} = \sigma_{ji} = \lambda\varepsilon_{kk}\delta_{ij} + 2\mu\varepsilon_{ij} \tag{3a}$$

$$\tau_{ijk} = \tau_{ikj} = \frac{1}{2}a_1(\xi_{kpp}\delta_{ij} + 2\xi_{ppi}\delta_{jk} + \xi_{jpp}\delta_{ik}) + 2a_2\xi_{ipp}\delta_{jk} + a_3(\xi_{ppk}\delta_{ij} + \xi_{ppj}\delta_{ik}) + 2a_4\xi_{ijk} + a_5(\xi_{jki} + \xi_{kji}) \tag{3b}$$

where δ_{ij} is the Kronecker delta. In the constitutive equation of the classical stress σ, the parameters $\lambda = Ev/[(1+v)(1-2v)]$ and $\mu = E/[2(1+v)]$ are Lame parameters [47].

3. GOVERNING EQUATIONS

Consider an FG microbeam made of a mixture of ceramic and metal with length L and thickness h. A coordinate system x y z is introduced on the central axis of the microbeam, where the x axis is taken along the length of the microbeam, the y axis in the width direction and the z axis is taken along the height direction. Also, the origin of the coordinate system is selected at the left end of the microbeam. The materials at bottom ($z = -h/2$) and top ($z = +h/2$) surfaces of the microbeam are considered to be ceramic-rich and metal-rich, respectively. The volume fractions of ceramic (V_c) and metal (V_m) phases can be defined by the following simple power law functions

$$V_c(z) = \left(\frac{1}{2} + \frac{z}{h}\right)^k, \quad V_m(z) = 1 - \left(\frac{1}{2} + \frac{z}{h}\right)^k \tag{4}$$

where k denotes the material gradient index. Effective Young's modulus (E), Poisson's ratio (v) and mass density (ρ) of FG microbeam are given as

$$E(z) = E_cV_c + E_mV_m, \quad v(z) = v_cV_c + v_mV_m, \quad \rho(z) = \rho_cV_c + \rho_mV_m. \tag{5}$$

Based upon the Timoshenko beam theory, the displacements of an arbitrary point in the microbeam along the x-, y- and z-axes are equal to

$$u_1 = U(t,x) - z\Psi(t,x), \quad u_2 = 0, \quad u_3 = W(t,x) \tag{6}$$

https://doi.org/10.1017/jmech.2013.65 Published online by Cambridge University Press

where $U(t, x)$, $W(t, x)$ and $\Psi(t, x)$ are the axial displacement of the center of cross sections, lateral deflection, and rotation angle of the cross section with respect to the vertical direction. Assuming tiny slopes after deflection and possible finite transverse deflection W, the nonlinear strain-displacement relationship can be approximated by the von Karman relations as follows

$$\varepsilon_{xx}=\frac{\partial u_1}{\partial x}+\frac{1}{2}\left(\frac{\partial W}{\partial x}\right)^2=\frac{\partial U}{\partial x}-z\frac{\partial \Psi}{\partial x}+\frac{1}{2}\left(\frac{\partial W}{\partial x}\right)^2,$$
$$\varepsilon_{xz}=\frac{1}{2}\left(\frac{\partial W}{\partial x}-\Psi\right) \tag{7}$$

By substituting Eqs. (6) and (7) into Eq. (2b), the nonzero components of ξ are obtained as

$$\xi_{xxx}=\frac{\partial^2 U}{\partial x^2}+\frac{\partial W}{\partial x}\frac{\partial^2 W}{\partial x^2}-z\frac{\partial^2 \Psi}{\partial x^2},$$
$$\xi_{xxz}=\xi_{xzx}=\frac{1}{2}\left(\frac{\partial^2 W}{\partial x^2}-\frac{\partial \Psi}{\partial x}\right),\ \xi_{zxx}=-\frac{\partial \Psi}{\partial x}. \tag{8}$$

The major constituents of the symmetric section of the stress tensor are expressed by

$$\sigma_{xx}=(\lambda+2\mu)\left[\frac{\partial U}{\partial x}-z\frac{\partial \Psi}{\partial x}+\frac{1}{2}\left(\frac{\partial W}{\partial x}\right)^2\right],$$
$$\sigma_{xz}=\mu k_s\left(\frac{\partial W}{\partial x}-\Psi\right). \tag{9}$$

where k_s is the shear correction factor. Inserting Eq. (8) into Eq. (3b) leads to the following nonzero components of the higher-order stresses

$$\tau_{xxx}=2(a_1+a_2+a_3+a_4+a_5)\left(\frac{\partial^2 U}{\partial x^2}+\frac{\partial W}{\partial x}\frac{\partial^2 W}{\partial x^2}-z\frac{\partial^2 \Psi}{\partial x^2}\right),$$
$$\tau_{xxz}=\tau_{xzx}=\frac{1}{2}(a_3+2a_4+a_5)\frac{\partial^2 W}{\partial x^2}-\frac{1}{2}(a_1+a_3+2a_4+3a_5)\frac{\partial \Psi}{\partial x},$$
$$\tau_{zxx}=\frac{1}{2}(a_1+2a_5)\frac{\partial^2 W}{\partial x^2}-\frac{1}{2}(a_1+4a_2+4a_4+2a_5)\frac{\partial \Psi}{\partial x}. \tag{10}$$

By substituting Eqs. (7) ~ (10) into Eq. (1), the strain energies corresponding to the classical theory (Π_C) and strain gradient theory (Π_{NC}) are derived as

$$\Pi_C=\frac{1}{2}\int_V \sigma:\varepsilon dV=\frac{1}{2}\int_0^L\left\{N_{xx}\left[\frac{\partial U}{\partial x}+\frac{1}{2}\left(\frac{\partial W}{\partial x}\right)^2\right]-M_{xx}\frac{\partial \Psi}{\partial x}+Q\left(\frac{\partial W}{\partial x}-\Psi\right)\right\}dx \tag{11a}$$

$$\Pi_{NC}=\frac{1}{2}\int_V \tau:\xi dV=\frac{1}{2}\int_0^L\left\{T_{xxx}\left(\frac{\partial^2 U}{\partial x^2}+\frac{\partial W}{\partial x}\frac{\partial^2 W}{\partial x^2}\right)-M_{xxx}\frac{\partial^2 \Psi}{\partial x^2}+T_{xxz}\left(\frac{\partial^2 W}{\partial x^2}-\frac{\partial \Psi}{\partial x}\right)-T_{zxx}\frac{\partial \Psi}{\partial x}\right\}dx \tag{11b}$$

Strain energy as a result of the variation of classical and higher order stresses with respect to the initial configuration can be given by $\Pi_s=\Pi_C+\Pi_{NC}$. In Eq. (11), the normal resultant force N_{xx}, shear force Q, bending moment M_{xx} and the other higher-order resultant forces and higher order moments (T_{xxx} M_{xxx} T_{xxz} T_{zxx}), due to higher-order stresses acting on a section can be obtained by

$$\{N_{xx}, Q, T_{xxx}, T_{xxz}, T_{zxx}\}=\int_A\{\sigma_{xx}, \sigma_{xz}, \tau_{xxx}, \tau_{xxz}, \tau_{zxx}\}\,dA,$$
$$\{M_{xx}, M_{xxx}\}=\int_A\{\sigma_{xx}, \tau_{xxx}\}\,zdA \tag{12}$$

In addition, the kinetic energy of microbeam, Π_T, is written as

$$\Pi_T=\frac{1}{2}\int_0^L\int_A\rho\left\{\left(\frac{\partial U}{\partial t}-z\frac{\partial \Psi}{\partial t}\right)^2+\left(\frac{\partial W}{\partial t}\right)^2\right\}dAdx$$
$$=\frac{1}{2}\int_0^L\left\{I_1\left(\frac{\partial U}{\partial t}\right)^2-2I_2\frac{\partial U}{\partial t}\frac{\partial \Psi}{\partial t}+I_3\left(\frac{\partial \Psi}{\partial t}\right)^2+I_1\left(\frac{\partial W}{\partial t}\right)^2\right\}dx \tag{13}$$

where ρ and A are the density and cross-sectional area of the microbeam, respectively. The inertia terms appeared in Eq. (13) are given by

$$\{I_1,\ I_2,\ I_3\}=\int_{-h/2}^{h/2}\rho(z)\{1,\ z,\ z^2\}\,dz. \tag{14}$$

Based on Hamilton's principle, *i.e.* $\delta\int_{t_1}^{t_2}(\Pi_T-\Pi_s)\,dt=0$, the following governing equations and associated boundary conditions are derived

$$\frac{\partial N_{xx}}{\partial x}-\frac{\partial^2 T_{xxx}}{\partial x^2}=I_1\frac{\partial^2 U}{\partial t^2}-I_2\frac{\partial^2 \Psi}{\partial t^2}, \tag{15a}$$

$$\frac{\partial}{\partial x}\left(N_{xx}\frac{\partial w}{\partial x}-\frac{\partial T_{xxx}}{\partial x}\frac{\partial w}{\partial x}\right)+\frac{\partial Q}{\partial x}-\frac{\partial^2 T_{xxz}}{\partial x^2}=I_1\frac{\partial^2 W}{\partial t^2}, \tag{15b}$$

$$Q-\frac{\partial(M_{xx}+T_{xxz}+T_{zxx})}{\partial x}+\frac{\partial^2 M_{xxx}}{\partial x^2}=I_3\frac{\partial^2 \Psi}{\partial t^2}-I_2\frac{\partial^2 U}{\partial t^2}. \tag{15c}$$

$$\left(N_{xx}-\frac{\partial T_{xxx}}{\partial x}\right)\Big|_{x=0,L}=0\quad or\quad \delta U\big|_{x=0,L}=0, \tag{15d}$$

$$\left(N_{xx}\frac{\partial W}{\partial x}+Q-\frac{\partial T_{xxx}}{\partial x}\frac{\partial W}{\partial x}+\frac{\partial T_{xxz}}{\partial x}\right)\Big|_{x=0,L}=0\quad \text{or}\quad \delta W\big|_{x=0,L}=0, \tag{15e}$$

$$\left(M_{xx}+T_{xxz}+T_{zxx}-\frac{\partial M_{xxx}}{\partial x}\right)\Big|_{x=0,L}=0\quad \text{or}\quad \delta\Psi\big|_{x=0,L}=0 \tag{15f}$$

$$T_{xxx}\big|_{x=0,L}=0\ \text{or}\ \delta\left(\frac{\partial U}{\partial x}\right)\Big|_{x=0,L}=0 \tag{15g}$$

https://doi.org/10.1017/jmech.2013.65 Published online by Cambridge University Press

$$\left(T_{xxx}\frac{\partial W}{\partial x}+T_{xxz}\right)\Big|_{x=0,L}=0 \quad \text{or} \quad \delta\left(\frac{\partial W}{\partial x}\right)\Big|_{x=0,L}=0 \tag{15h}$$

$$M_{xxx}\big|_{x=0,L}=0 \quad \text{or} \quad \delta\left(\frac{\partial \Psi}{\partial x}\right)\Big|_{x=0,L}=0 \tag{15i}$$

Consider the following parameters

$$\begin{aligned}
&\{A_{11},B_{11},D_{11}\}=\int_{-h/2}^{h/2}(\lambda+2\mu)\{1,z,z^2\}\,dz\,,\\
&A_{22}=-\frac{1}{2}\int_{-h/2}^{h/2}(a_1+a_3+2a_4+3a_5)\,dz\,,\\
&\{A_{33},B_{33},D_{33}\}=2\int_{-h/2}^{h/2}(a_1+a_2+a_3+a_4+a_5)\{1,z,z^2\}\,dz\,,\\
&A_{44}=\frac{1}{2}\int_{-h/2}^{h/2}(a_5+2a_4+a_3)\,dz\,,\\
&\{A_{55},B_{55},D_{55}\}=\int_{-h/2}^{h/2}\mu\{1,z,z^2\}\,dz\,,\\
&A_{66}=\frac{1}{2}\int_{-h/2}^{h/2}(2a_1+5a_5+a_3+6a_4+4a_2)\,dz\,.
\end{aligned} \tag{16}$$

Also, consider the following dimensionless parameters

$$\zeta=\frac{x}{L},\quad \eta=\frac{L}{h},\quad (u,w)=\frac{(U,W)}{h},\quad \psi=\Psi,\quad \tau=\frac{t}{L}\sqrt{\frac{A_{110}}{I_{10}}} \tag{17a}$$

$$\begin{aligned}
&(a_{11},\,a_{55},b_{11},\,b_{55},,d_{11},\,d_{55})\\
&\quad=\left(\frac{A_{11}}{A_{110}},\frac{A_{55}}{A_{110}},\frac{B_{11}}{A_{110}h},\frac{B_{55}}{A_{110}h},\frac{D_{11}}{A_{110}h^2},\frac{D_{55}}{A_{110}h^2}\right),\\
&(a_{22},\,a_{44},\,a_{66})=\left(\frac{A_{22}}{A_{110}h^2},\frac{A_{44}}{A_{110}h^2},\frac{A_{66}}{A_{110}h^2}\right),\\
&(a_{33},\,a_{33},\,a_{33})=\left(\frac{A_{33}}{A_{110}h^2},\frac{B_{33}}{A_{110}h^3},\frac{D_{33}}{A_{110}h^4}\right),
\end{aligned} \tag{17b}$$

$$(\bar{I}_1,\,\bar{I}_2,\,\bar{I}_3)=\left(\frac{I_1}{I_{10}},\frac{I_2}{I_{10}h},\frac{I_3}{I_{10}h^2}\right), \tag{17c}$$

where A_{110} and I_{10} are the values of A_{11} and I_1 for a homogeneous beam made of metal. Via Eq. (17), the dimensionless governing equations together with the dimensionless boundary conditions can be expressed as

$$\begin{aligned}
&a_{11}\left(\frac{\partial^2 u}{\partial\zeta^2}+\frac{1}{\eta}\frac{\partial w}{\partial\zeta}\frac{\partial^2 w}{\partial\zeta^2}\right)\\
&-b_{11}\frac{\partial^2\psi}{\partial\zeta^2}-\frac{a_{33}}{\eta^2}\left(\frac{\partial^4 u}{\partial\zeta^4}+\frac{1}{\eta}\frac{\partial w}{\partial\zeta}\frac{\partial^4 w}{\partial\zeta^4}+\frac{3}{\eta}\frac{\partial^2 w}{\partial x^2}\frac{\partial^3 w}{\partial x^3}\right)\\
&+\frac{b_{33}}{\eta^2}\frac{\partial^4\psi}{\partial\zeta^4}=\bar{I}_1\frac{\partial^2 u}{\partial\tau^2}-\bar{I}_2\frac{\partial^2\psi}{\partial\tau^2}\,,
\end{aligned} \tag{18a}$$

$$\begin{aligned}
&k_s a_{55}\left(\frac{\partial^2 w}{\partial\zeta^2}-\eta\frac{\partial\psi}{\partial\zeta}\right)-\frac{a_{44}}{\eta^2}\frac{\partial^4 w}{\partial\zeta^4}-\frac{a_{22}}{\eta}\frac{\partial^3\psi}{\partial\zeta^3}\\
&+\frac{a_{11}}{\eta}\left[\frac{\partial u}{\partial\zeta}\frac{\partial^2 w}{\partial\zeta^2}+\frac{\partial^2 u}{\partial\zeta^2}\frac{\partial w}{\partial\zeta}+\frac{3}{2\eta}\frac{\partial^2 w}{\partial\zeta^2}\left(\frac{\partial w}{\partial\zeta}\right)^2\right]\\
&-\frac{b_{11}}{\eta}\left(\frac{\partial\psi}{\partial\zeta}\frac{\partial^2 w}{\partial\zeta^2}+\frac{\partial w}{\partial\zeta}\frac{\partial^2\psi}{\partial\zeta^2}\right)-\frac{a_{33}}{\eta^3}\left(\frac{\partial^4 u}{\partial\zeta^4}\frac{\partial w}{\partial\zeta}+\frac{\partial^3 u}{\partial\zeta^3}\frac{\partial^2 w}{\partial\zeta^2}\right)\\
&+\frac{b_{33}}{\eta^3}\left(\frac{\partial w}{\partial\zeta}\frac{\partial^4\psi}{\partial\zeta^4}+\frac{\partial^2 w}{\partial\zeta^2}\frac{\partial^3\psi}{\partial\zeta^3}\right)\\
&-\frac{a_{33}}{\eta^4}\left[4\frac{\partial w}{\partial\zeta}\frac{\partial^2 w}{\partial\zeta^2}\frac{\partial^3 w}{\partial\zeta^3}+\frac{\partial^4 w}{\partial\zeta^4}\left(\frac{\partial w}{\partial\zeta}\right)^2+\left(\frac{\partial^2 w}{\partial\zeta^2}\right)^3\right]=\bar{I}_1\frac{\partial^2 w}{\partial\tau^2}\,,
\end{aligned} \tag{18b}$$

$$\begin{aligned}
&k_s a_{55}\eta\left(\frac{\partial w}{\partial\zeta}-\eta\psi\right)-b_{11}\left(\frac{\partial^2 u}{\partial\zeta^2}+\frac{1}{\eta}\frac{\partial w}{\partial\zeta}\frac{\partial^2 w}{\partial\zeta^2}\right)\\
&+d_{11}\frac{\partial^2\psi}{\partial\zeta^2}-\frac{d_{33}}{\eta^2}\frac{\partial^4\psi}{\partial\zeta^4}+\frac{a_{22}}{\eta}\frac{\partial^3 w}{\partial\zeta^3}+a_{66}\frac{\partial^2\psi}{\partial\zeta^2}\\
&+\frac{b_{33}}{\eta^2}\left(\frac{\partial^4 u}{\partial\zeta^4}+\frac{1}{\eta}\frac{\partial w}{\partial\zeta}\frac{\partial^4 w}{\partial\zeta^4}+\frac{3}{\eta}\frac{\partial^2 w}{\partial\zeta^2}\frac{\partial^3 w}{\partial\zeta^3}\right)=\bar{I}_3\frac{\partial^2\psi}{\partial\tau^2}-\bar{I}_2\frac{\partial^2 u}{\partial\tau^2}\,.
\end{aligned} \tag{18c}$$

$$\begin{aligned}
&\delta u\big|_{\zeta=0,1}=0 \;\; or\\
&\left\{a_{11}\left[\frac{\partial u}{\partial\zeta}+\frac{1}{2\eta}\left(\frac{\partial w}{\partial\zeta}\right)^2\right]-b_{11}\frac{\partial\psi}{\partial\zeta}\right.\\
&\left.-\frac{a_{33}}{\eta^2}\left[\frac{\partial^3 u}{\partial\zeta^3}+\frac{1}{\eta}\frac{\partial w}{\partial\zeta}\frac{\partial^3 w}{\partial\zeta^3}+\frac{1}{\eta}\left(\frac{\partial^2 w}{\partial\zeta^2}\right)^2\right]+\frac{b_{33}}{\eta^2}\frac{\partial^3\psi}{\partial\zeta^3}\right\}\Bigg|_{\zeta=0,1}=0
\end{aligned} \tag{18d}$$

$$\delta\left(\frac{\partial u}{\partial\zeta}\right)\Big|_{\zeta=0,L}=0 \;\; \text{or} \;\; \left\{a_{33}\left(\frac{\partial^2 u}{\partial\zeta^2}+\frac{1}{\eta}\frac{\partial w}{\partial\zeta}\frac{\partial^2 w}{\partial\zeta^2}\right)-b_{33}\frac{\partial^2\psi}{\partial\zeta^2}\right\}\Big|_{\zeta=0,1}=0\,, \tag{18e}$$

$$\begin{aligned}
&\delta w\big|_{\zeta=0,1}=0 \;\; \text{or}\left\{k_s a_{55}\left(\frac{\partial w}{\partial\zeta}-\eta\psi\right)+\frac{a_{11}}{\eta}\left[\frac{\partial u}{\partial\zeta}\frac{\partial w}{\partial\zeta}+\frac{1}{2\eta}\left(\frac{\partial w}{\partial\zeta}\right)^3\right]\right.\\
&-\frac{b_{11}}{\eta}\frac{\partial\psi}{\partial\zeta}\frac{\partial w}{\partial\zeta}+\frac{a_{44}}{\eta^2}\frac{\partial^3 w}{\partial\zeta^3}+\frac{a_{22}}{\eta}\frac{\partial^2\psi}{\partial\zeta^2}-\frac{a_{33}}{\eta^3}\left[\frac{\partial^3 u}{\partial\zeta^3}\frac{\partial w}{\partial\zeta}+\frac{1}{\eta}\left(\frac{\partial w}{\partial\zeta}\right)^2\frac{\partial^3 w}{\partial\zeta^3}\right.\\
&\left.\left.+\frac{1}{\eta}\frac{\partial w}{\partial\zeta}\left(\frac{\partial^2 w}{\partial\zeta^2}\right)^2\right]+\frac{b_{33}}{\eta^3}\frac{\partial^3\psi}{\partial\zeta^3}\frac{\partial w}{\partial\zeta}\right\}\Bigg|_{\zeta=0,1}=0\,,
\end{aligned} \tag{18f}$$

$$\begin{aligned}
&\delta\left(\frac{\partial w}{\partial\zeta}\right)\Big|_{\zeta=0,1}=0\\
&\text{or}\left\{a_{44}\frac{\partial^2 w}{\partial\zeta^2}+a_{22}\eta\frac{\partial\psi}{\partial\zeta}+\frac{a_{33}}{\eta}\left(\frac{\partial^2 u}{\partial\zeta^2}+\frac{1}{\eta}\frac{\partial w}{\partial\zeta}\frac{\partial^2 w}{\partial\zeta^2}\right)\frac{\partial w}{\partial\zeta}\right.\\
&\left.-\frac{b_{33}}{\eta}\frac{\partial^2\psi}{\partial\zeta^2}\frac{\partial w}{\partial\zeta}\right\}\Bigg|_{\zeta=0,1}=0\,,
\end{aligned} \tag{18g}$$

https://doi.org/10.1017/jmech.2013.65 Published online by Cambridge University Press

$$\delta\psi\big|_{\zeta=0,1}=0$$

$$\text{or}\ \left\{b_{11}\left[\frac{\partial u}{\partial\zeta}+\frac{1}{2\eta}\left(\frac{\partial w}{\partial\zeta}\right)^2\right]-d_{11}\frac{\partial\psi}{\partial\zeta}\right.$$
$$-\frac{b_{33}}{\eta^2}\left[\frac{\partial^3 u}{\partial\zeta^3}+\frac{1}{\eta}\frac{\partial w}{\partial\zeta}\frac{\partial^3 w}{\partial\zeta^3}+\frac{1}{\eta}\left(\frac{\partial^2 w}{\partial\zeta^2}\right)^2\right]$$
$$\left.+\frac{d_{33}}{\eta^2}\frac{\partial^3\psi}{\partial\zeta^3}-\frac{a_{22}}{\eta}\frac{\partial^2 w}{\partial\zeta^2}-a_{66}\frac{\partial\psi}{\partial\zeta}\right\}\Bigg|_{\zeta=0,1}=0 \qquad (18h)$$

$$\delta\left(\frac{\partial\psi}{\partial\zeta}\right)\Bigg|_{\zeta=0,1}=0$$

$$\text{or}\ \left\{b_{33}\left(\frac{\partial^2 u}{\partial\zeta^2}+\frac{1}{\eta}\frac{\partial w}{\partial\zeta}\frac{\partial^2 w}{\partial\zeta^2}\right)-d_{33}\frac{\partial^2\psi}{\partial\zeta^2}\right\}\Bigg|_{\zeta=0,1}=0 \qquad (18i)$$

The simply-supported boundary condition is given by

$$u=a_{33}\left(\frac{\partial^2 u}{\partial\zeta^2}+\frac{1}{\eta}\frac{\partial w}{\partial\zeta}\frac{\partial^2 w}{\partial\zeta^2}\right)-b_{33}\frac{\partial^2\psi}{\partial\zeta^2}=0,$$

$$w=a_{44}\frac{\partial^2 w}{\partial\zeta^2}+a_{22}\eta\frac{\partial\psi}{\partial\zeta}$$
$$+\frac{a_{33}}{\eta}\left(\frac{\partial^2 u}{\partial\zeta^2}+\frac{1}{\eta}\frac{\partial w}{\partial\zeta}\frac{\partial^2 w}{\partial\zeta^2}\right)\frac{\partial w}{\partial\zeta}-\frac{b_{33}}{\eta}\frac{\partial^2\psi}{\partial\zeta^2}\frac{\partial w}{\partial\zeta}=0,$$

$$b_{11}\left[\frac{\partial u}{\partial\zeta}+\frac{1}{2\eta}\left(\frac{\partial w}{\partial\zeta}\right)^2\right]-d_{11}\frac{\partial\psi}{\partial\zeta}+\frac{d_{33}}{\eta^2}\frac{\partial^3\psi}{\partial\zeta^3}-\frac{a_{22}}{\eta}\frac{\partial^2 w}{\partial\zeta^2}$$
$$-a_{66}\frac{\partial\psi}{\partial\zeta}-\frac{b_{33}}{\eta^2}\left[\frac{\partial^3 u}{\partial\zeta^3}+\frac{1}{\eta}\frac{\partial w}{\partial\zeta}\frac{\partial^3 w}{\partial\zeta^3}+\frac{1}{\eta}\left(\frac{\partial^2 w}{\partial\zeta^2}\right)^2\right]=0,$$

$$b_{33}\left(\frac{\partial^2 u}{\partial\zeta^2}+\frac{1}{\eta}\frac{\partial w}{\partial\zeta}\frac{\partial^2 w}{\partial\zeta^2}\right)-d_{33}\frac{\partial^2\psi}{\partial\zeta^2}=0. \qquad (19)$$

and clamped boundary condition is expressed as

$$u=0,\ w=0,\ \psi=0,\ \frac{\partial u}{\partial\zeta}=0,\ \frac{\partial w}{\partial\zeta}=0,\ \frac{\partial\psi}{\partial\zeta}=0. \qquad (20)$$

By considering the following parameters

$$a_1=\mu\left(l_2^2-\frac{4}{15}l_1^2\right),\ a_2=\mu\left(l_0^2-\frac{1}{15}l_1^2-\frac{1}{2}l_2^2\right),$$
$$a_3=-\mu\left(\frac{4}{15}l_1^2+\frac{1}{2}l_2^2\right),$$
$$a_4=\mu\left(\frac{1}{3}l_1^2+l_2^2\right),\ a_5=\mu\left(\frac{2}{3}l_1^2-l_2^2\right). \qquad (21)$$

in which l_0, l_1 and l_2 show the independent material length scale parameters respectively associated with the dilatation gradients, deviatoric stretch gradients and symmetric rotation gradients, the current most general form of strain gradient beam model can be reduced to the nonlinear FG Timoshenko beam model based on the MSGT [25]. Moreover, when $l_0 = l_1 = 0$ the present model is reduced to the model of MCST [24], and it is reduced to the classical theory when all material length scale parameters become equal to zero.

4. SOLUTION METHODOLOGY

4.1 Discretized Equations

In this subsection, the GDQ method [48] is employed to derive the discretized counterparts of governing equations together with the boundary conditions. First, grid points in ξ_i direction are generated using the shifted Chebyshev–Gauss–Lobatto grid points, given by

$$\xi_i=\frac{1}{2}\left(1-\cos\frac{i-1}{N-1}\pi\right),\quad i=1,2,\ldots,N \qquad (22)$$

Column vectors **U**, **W** and **Ψ** are defined as

$$\mathbf{U}=\{U_1,U_2,\ldots,U_N\}^T,\ \mathbf{W}=\{W_1,W_2,\ldots,W_N\}^T,$$
$$\mathbf{\Psi}=\{\Psi_1,\Psi_2,\ldots,\Psi_N\}^T, \qquad (23)$$

with N entries equal to the number of grid points $U_i = u(\xi_i)$ $W_i = w(\xi_i)$ and $\Psi_i = \psi(\xi_i)$. The discretized form of governing equations given by Eqs. 18(a) ~ 18(c) can be shown by

$$\mathbf{M}\ddot{\mathbf{X}}+\mathbf{K}\mathbf{X}+\mathbf{N}(\mathbf{X})=0 \qquad (24)$$

in which field variables vector **X,** stiffness matrix **K,** mass matrix **M** and nonlinear part vector **N**(**X**) are given as

$$\mathbf{X}=\{\mathbf{U}^{\mathrm{T}},\mathbf{W}^{\mathrm{T}},\mathbf{\Psi}^{\mathrm{T}}\}^{\mathrm{T}} \qquad (25a)$$

$$\mathbf{M}=\begin{bmatrix}-\bar{I}_1\mathbf{D}_\xi^{(0)} & 0 & \bar{I}_2\mathbf{D}_\xi^{(0)}\\ 0 & -\bar{I}_1\mathbf{D}_\xi^{(0)} & 0\\ \bar{I}_2\mathbf{D}_\xi^{(0)} & 0 & -\bar{I}_3\mathbf{D}_\xi^{(0)}\end{bmatrix} \qquad (25b)$$

https://doi.org/10.1017/jmech.2013.65 Published online by Cambridge University Press

$$\mathbf{K}=\begin{bmatrix} a_{11}\mathbf{D}_\xi^{(2)}-\dfrac{a_{33}}{\eta^2}\mathbf{D}_\xi^{(4)} & 0 & -b_{11}\mathbf{D}_\xi^{(2)}+\dfrac{b_{33}}{\eta^2}\mathbf{D}_\xi^{(4)} \\ 0 & k_s a_{55}\mathbf{D}_\xi^{(2)}-\dfrac{a_{44}}{\eta^2}\mathbf{D}_\xi^{(4)} & -k_s a_{55}\eta\mathbf{D}_\xi^{(1)}-\dfrac{a_{22}}{\eta}\mathbf{D}_\xi^{(3)} \\ -b_{11}\mathbf{D}_\xi^{(2)}+\dfrac{b_{33}}{\eta^2}\mathbf{D}_\xi^{(4)} & k_s a_{55}\eta\mathbf{D}_\xi^{(1)}+\dfrac{a_{22}}{\eta}\mathbf{D}_\xi^{(3)} & -k_s a_{55}\eta^2\mathbf{D}_\xi^{(0)}+(a_{66}+d_{11})\mathbf{D}_\xi^{(2)}-\dfrac{d_{33}}{\eta^2}\mathbf{D}_\xi^{(4)} \end{bmatrix} \tag{25c}$$

$$\mathbf{N}(\mathbf{X})=\left\{\mathbf{N}_\mathbf{u}(\mathbf{X})^{\mathrm{T}},\mathbf{N}_\mathbf{w}(\mathbf{X})^{\mathrm{T}},\mathbf{N}_\boldsymbol{\psi}(\mathbf{X})^{\mathrm{T}}\right\}^{\mathrm{T}},$$

$$\begin{aligned}\mathbf{N}_\mathbf{u}(\mathbf{X})&=a_{11}\frac{1}{\eta}(\mathbf{D}_\xi^{(1)}\mathbf{W})\circ(\mathbf{D}_\xi^{(2)}\mathbf{W})\\&\quad-\frac{a_{33}}{\eta^2}\left(\frac{1}{\eta}(\mathbf{D}_\xi^{(1)}\mathbf{W})\circ(\mathbf{D}_\xi^{(4)}\mathbf{W})+\frac{3}{\eta}(\mathbf{D}_\xi^{(2)}\mathbf{W})\circ(\mathbf{D}_\xi^{(3)}\mathbf{W})\right),\\ \mathbf{N}_\mathbf{w}(\mathbf{X})&=\frac{a_{11}}{\eta}\left((\mathbf{D}_\xi^{(1)}\mathbf{U})\circ(\mathbf{D}_\xi^{(2)}\mathbf{W})+(\mathbf{D}_\xi^{(2)}\mathbf{U})\circ(\mathbf{D}_\xi^{(1)}\mathbf{W})+\frac{3}{2\eta}(\mathbf{D}_\xi^{(2)}\mathbf{W})\circ(\mathbf{D}_\xi^{(1)}\mathbf{W})\circ(\mathbf{D}_\xi^{(1)}\mathbf{W})\right)\\&\quad-\frac{b_{11}}{\eta}\left((\mathbf{D}_\xi^{(1)}\boldsymbol{\Psi})\circ(\mathbf{D}_\xi^{(2)}\mathbf{W})+(\mathbf{D}_\xi^{(1)}\mathbf{W})\circ(\mathbf{D}_\xi^{(2)}\boldsymbol{\Psi})\right)-\frac{a_{33}}{\eta^3}\left((\mathbf{D}_\xi^{(4)}\mathbf{U})\circ(\mathbf{D}_\xi^{(1)}\mathbf{W})+(\mathbf{D}_\xi^{(3)}\mathbf{U})\circ(\mathbf{D}_\xi^{(2)}\mathbf{W})\right)\\&\quad-\frac{a_{33}}{\eta^4}\left(4(\mathbf{D}_\xi^{(1)}\mathbf{W})\circ(\mathbf{D}_\xi^{(2)}\mathbf{W})\circ(\mathbf{D}_\xi^{(3)}\mathbf{W})+(\mathbf{D}_\xi^{(4)}\mathbf{W})\circ(\mathbf{D}_\xi^{(1)}\mathbf{W})\circ(\mathbf{D}_\xi^{(1)}\mathbf{W})+(\mathbf{D}_\xi^{(2)}\mathbf{W})\circ(\mathbf{D}_\xi^{(2)}\mathbf{W})\circ(\mathbf{D}_\xi^{(2)}\mathbf{W})\right)\\&\quad+\frac{b_{33}}{\eta^3}\left((\mathbf{D}_\xi^{(1)}\mathbf{W})\circ(\mathbf{D}_\xi^{(4)}\boldsymbol{\Psi})+(\mathbf{D}_\xi^{(2)}\mathbf{W})\circ(\mathbf{D}_\xi^{(3)}\boldsymbol{\Psi})\right),\\ \mathbf{N}_\boldsymbol{\psi}(\mathbf{X})&=-\frac{1}{\eta}(\mathbf{D}_\xi^{(1)}\mathbf{W})\circ(\mathbf{D}_\xi^{(2)}\mathbf{W})+\frac{b_{33}}{\eta^2}\left(\frac{1}{\eta}(\mathbf{D}_\xi^{(1)}\mathbf{W})\circ(\mathbf{D}_\xi^{(4)}\mathbf{W})+\frac{3}{\eta}(\mathbf{D}_\xi^{(2)}\mathbf{W})\circ(\mathbf{D}_\xi^{(3)}\mathbf{W})\right).\end{aligned} \tag{25d}$$

where $\circ$ shows the Hadamard product whose definition together with the weighting coefficients of the first and higher-order derivatives can be found in Appendix A. The boundary conditions can be discretized, similarly. For instance, in the case of clamped ends, the discretized form of Eq. (20) is

$$\mathbf{U}=\mathbf{W}=\boldsymbol{\Psi}=\mathbf{D}_\xi^{(1)}\mathbf{U}=\mathbf{D}_\xi^{(1)}\mathbf{W}=\mathbf{D}_\xi^{(1)}\boldsymbol{\Psi}=0 \ \text{ at } \ \xi=0,1. \tag{26}$$

4.2 Numerical Galerkin Approach

Here, a Galerkin-based numerical approach is applied in order to reduce the set of nonlinear equations of (24) into a time-varying set of ordinary differential equations of Duffing-type. Assuming a harmonic solution, $\mathbf{X}=\tilde{\mathbf{X}}e^{j\omega t}$, and by dropping the nonlinear terms in Eq. (24), the following general eigenvalue problem can be obtained

$$\mathbf{K}\tilde{\mathbf{X}}=-\omega^2\mathbf{M}\tilde{\mathbf{X}} \tag{27}$$

It should be noted that the elements of discretized boundary conditions equivalent to boundary nodes must be replaced with the same elements in the matrix equation of (27). After solving Eq. (27) and obtaining linear mode shapes, the solution of Eq. (24) is considered as

$$\mathbf{X}=\boldsymbol{\Phi}\mathbf{q} \tag{28}$$

where $\mathbf{q}$ and $\boldsymbol{\Phi}$ are the reduced generalized coordinates and basis functions used in the numerical Galerkin method (a sparse matrix which contains the first m eigenvectors), respectively. They are given by

$$\mathbf{q}^{T}{}_{(3m)\times1}=\{q_u^1,q_u^2,\ldots,q_u^m,q_w^1,q_w^2,\ldots,q_w^m,q_\psi^1,q_\psi^2,\ldots,q_\psi^m\} \tag{29a}$$

$$\boldsymbol{\Phi}_{(3N)\times(3m)}=\begin{bmatrix}\boldsymbol{\Phi}_\mathbf{u} & \mathbf{0} & \mathbf{0}\\ \mathbf{0} & \boldsymbol{\Phi}_\mathbf{w} & \mathbf{0}\\ \mathbf{0} & \mathbf{0} & \boldsymbol{\Phi}_\boldsymbol{\psi}\end{bmatrix} \tag{29b}$$

where

$$\boldsymbol{\Phi}_{uN\times m}=\left[\{\tilde{X}_u^1\}_{N\times1},\ldots,\{\tilde{X}_u^m\}_{N\times1}\right] \tag{30a}$$

$$\boldsymbol{\Phi}_{wN\times m}=\left[\{\tilde{X}_w^1\}_{N\times1},\ldots,\{\tilde{X}_w^m\}_{N\times1}\right] \tag{30b}$$

$$\boldsymbol{\Phi}_{\psi N\times m}=\left[\{\tilde{X}_\psi^1\}_{N\times1},\ldots,\{\tilde{X}_\psi^m\}_{N\times1}\right] \tag{30c}$$

By substituting Eq. (28) into Eq. (24) the residual can be obtained as follows

$$\mathbf{R}=\mathbf{M}\boldsymbol{\Phi}\ddot{\mathbf{q}}+\mathbf{K}\boldsymbol{\Phi}\mathbf{q}+\mathbf{N}(\boldsymbol{\Phi}\mathbf{q}) \tag{31}$$

Multiplying each equation by corresponding mode shapes and integrating over the domain in the numerical Galerkin approach can be simultaneously performed via the following matrix operator

$$\mathbf{G}_{m\times3N}=(\mathbf{S}\lozenge\boldsymbol{\Phi}^{\mathrm{T}}),\ \mathbf{S}=\{\mathbf{S}_\xi,\mathbf{S}_\xi,\mathbf{S}_\xi\}_{1\times(3N)} \tag{32}$$

in which $\lozenge$ denotes the SJT product and $\mathbf{S}_\xi$ is the integral operator (see Appendixes A and B). By multiplying the operator of Eq. (32) by the residual vector of

https://doi.org/10.1017/jmech.2013.65 Published online by Cambridge University Press

Eq. (31) one can arrive at the reduced form of Eq. (24) as

$$\tilde{\mathbf{M}}\ddot{\mathbf{q}} + \tilde{\mathbf{K}}\mathbf{q} + \tilde{\mathbf{N}}(\mathbf{q}) = 0 \tag{33}$$

where

$$\tilde{\mathbf{M}} = \mathbf{G}\mathbf{M}\mathbf{\Phi}\ ,\ \ \tilde{\mathbf{K}} = \mathbf{G}\mathbf{K}\mathbf{\Phi}\ ,\ \ \tilde{\mathbf{N}}(\mathbf{q}) = \mathbf{G}\mathbf{N}(\mathbf{\Phi}\mathbf{q}) \tag{34}$$

It is found that the general coordinates are reduced from 3*N* discrete points into 3*m* ones (where *N* and *m* are the number of discrete points in the GDQ method and the number of chosen mode shapes in the Galerkin method, respectively). It must be noted that both essential and natural boundary conditions are satisfied in the present numerical Galerkin approach as the linear mode shapes used in the method are obtained from a numerical technique. Also, it is worth mentioning that the small scale effects are taken into consideration since the linear mode shapes used in the method are obtained from the strain gradient elasticity rather than from the classical elasticity. Hence, it can be concluded that by using the present numerical Galerkin method the desired accuracy is achieved via a small number of mode shapes and for this reason the computational expense significantly reduces. Using one mode shape, Eq. (33) is reduced to a three-degree-of-freedom coupled nonlinear Duffing oscillator as

$$\tilde{\mathbf{M}}\begin{Bmatrix}\ddot{q}_u\\ \ddot{q}_w\\ \ddot{q}_\psi\end{Bmatrix} + \tilde{\mathbf{K}}\begin{Bmatrix}q_u\\ q_w\\ q_\psi\end{Bmatrix} + \mathbf{G}\begin{bmatrix}0 & \mathbf{C}_1 & 0 & 0\\ \mathbf{C}_2 & 0 & \mathbf{C}_3 & \mathbf{C}_4\\ 0 & \mathbf{C}_5 & 0 & 0\end{bmatrix}\begin{Bmatrix}q_u q_w\\ (q_w)^2\\ q_w q_\psi\\ (q_w)^3\end{Bmatrix} = 0 \tag{35}$$

where $\boldsymbol{C}_i$ (i = 1, 2, …, 5) are directly associated with the basis function matrix $\mathbf{\Phi}$ (see Appendix C).

4.3 Time-Domain Solution

The harmonic balance method [49] can be used to reduce the set of nonlinear ordinary differential equations of (35) into a set of nonlinear algebraic equations. Based on the HBM, a set of algebraic equations is obtained through balancing the terms with the same frequency components. To this end, each time history is characterized by its frequency content. The steady-state response, $\mathbf{q} = \{q_u, q_w, q_\psi\}^{\mathrm{T}}$ for Eq. (35) is expressed as

$$\mathbf{q} = \sum_{i=1,3}^{2k-1} \mathbf{V}_i^c \cos i\Omega t + \mathbf{V}_i^s \sin i\Omega t\ ,\ \ \mathbf{V}_i = \{V_{ui}\ ,\ V_{w_i}\ ,\ V_{\psi i}\}^{\mathbf{T}} \tag{36}$$

where k is an integer number and denotes the number of harmonics. By inserting Eq. (36) into Eq. (35) one can obtain the following set of nonlinear algebraic equations

$$\mathbf{H}(\mathbf{V}_i^c, \mathbf{V}_i^s, \Omega) = 0,\ i = 1, 3, \ldots, 2k-1 \tag{37}$$

which is a mapping from $\mathbb{R}^{3(2k)+1} \to \mathbb{R}^{3(2k)}$. Note that in the HBM all nonlinear trigonometric functions are replaced with the linear ones. Here, only one harmonic (k = 1) is used that yields to a set of nonlinear equations $\mathbb{R}^7 \to \mathbb{R}^6$. The set of nonlinear equations of (37) can be considered as an eigenvalue problem in which Ω is the eigenvalue and $\{\mathbf{V}_i^c, \mathbf{V}_i^s\}^{\mathrm{T}}$ is the corresponding eigenvector. This problem cannot be solved using root finding method because Ω which is an eigenvalue cannot be considered as a parameter. Thus, a new parameter is introduced in the system by adding a normalizing equation as

$$\bar{\mathbf{H}} : \mathbb{R}^8 \to \mathbb{R}^7,$$
$$\bar{\mathbf{H}}(\mathbf{V}_i^c, \mathbf{V}_i^s, \Omega, c) = \begin{cases} H(\mathbf{V}_i^c, \mathbf{V}_i^s, \Omega) = 0 \\ \mathbf{V}_i^{c\mathrm{T}}\mathbf{V}_i^c + \mathbf{V}_i^{s\mathrm{T}}\mathbf{V}_i^s - c = 0 \end{cases} \tag{38}$$

Note that both $\{\mathbf{V}_i^c, \mathbf{V}_i^s\}^{\mathrm{T}}$ and Ω are related to the value of parameter c in the augmented system of (38). Finally, Eq. (38) can be solved using the Newton-Raphson method.

5. RESULTS AND DISCUSSION

In this section, numerical results are presented for the effects of material gradient index, length scale parameter, boundary conditions and length-to-thickness ratio on the nonlinear vibration of FG microbeams. It is assumed that the material of FG microbeams is a mixture of aluminum (Al) and ceramic (SiC) with the following material properties

E_m = 70GPa, ν_m = 0.3, ρ_m = 2702kg/m^3 for Al, and

E_c = 427GPa, ν_c = 0.17, ρ_c = 3100kg/m^3 for SiC.

The results are given for FG microbeams with three types of boundary conditions including simply supported-simply supported (SS), simply supported-clamped (SC) and clamped-clamped (CC). Furthermore, all results are generated for the case of MSGT (unless otherwise stated). It should be remarked that experimental data are required to obtain the length scale parameters of a homogeneous or FG microbeam. The length scale parameter of an isotropic homogeneous microbeam has been experimentally evaluated as l = 17.6μm in [25]. Nevertheless, to the best of the authors' knowledge, there are no available experimental data for the FG microbeams in the open literature. Thus, in order to quantitatively study the size effects on the nonlinear vibration behavior of FG microbeams, the values of length scale parameters are assumed to be equal ($l_0 = l_1 = l_2 = l$) and a dimensionless length scale parameter, h/l, is used for this purpose.

Figure 1 shows the variation of maximum of dimensionless transverse deflection ($W_{\max}/h$) versus the frequency ratio (Ω/ω_l) for FG microbeams with different material gradient indexes. It is observed that for all types of boundary conditions, both vibration amplitude

https://doi.org/10.1017/jmech.2013.65 Published online by Cambridge University Press

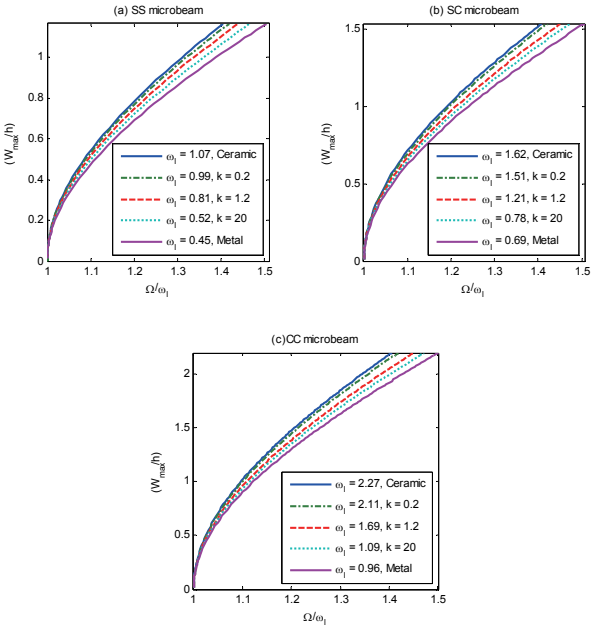


Fig. 1 Maximum of dimensionless transverse deflection versus frequency ratio for different gradient indexes ($\eta = 12$, $h/l = 2$)

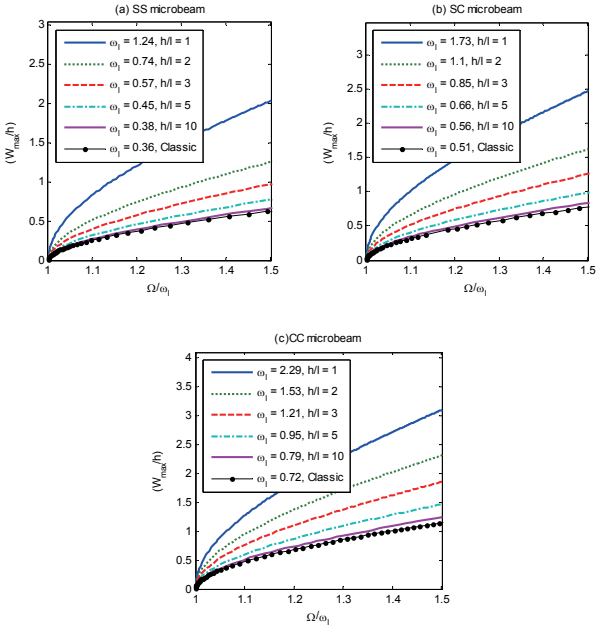


Fig. 2 Maximum of dimensionless transverse deflection versus frequency ratio for different dimensionless length scale parameters based on the MSGT ($\eta = 12$, $k = 2$)

and linear frequency decrease with the increase of the material gradient index. Also, it is seen that the nonlinear effects become more significant as the stiffness of material decreases.

The size effects on the nonlinear vibration of FG microbeams are shown in Figs. 2 and 3 based on the MSGT ($l_0 = l_1 = l_2 = l$) and MCST ($l_0 = l_1 = 0$, $l_2 = l$), respectively. The results of the classical theory ($l_0 = l_1 = l_2 = l$) are also presented in these figures. It is observed that the difference between the results obtained based on the MSGT and MCST, and those predicted by the classical theory is significant for small dimensionless length scale parameters and as h/l increases, the difference diminishes and the results of non-classical theories tend to those of classical theory. This observation can confirm the validity of the present numerical approach. It is worth mentioning that the convergence of the results obtained by the MCST to the results of classical theory is faster than that of the results obtained by the MSGT. One can see that by employing the MCST, the vibration amplitude is predicted smaller than that obtained by using the MSGT. Moreover, it is observed that with increasing the dimensionless length scale parameter, the vibration amplitude and linear frequency decrease. Figures 2 and 3 indicate that the importance of the small length scale is affected by the type of boundary conditions, so that the small scale effect is more pronounced for softer boundary conditions.

The effect of length-to-thickness ratio is illustrated in Fig. 4. This figure is presented to show the nonlinear vibration of FG microbeams at short lengths based on the Timoshenko beam theory. It is seen that as the length-to-thickness ratio becomes larger, the vibration amplitude and linear frequency respectively increases and decreases. Also, Fig. 5 shows the variation of maximum of dimensionless transverse deflection

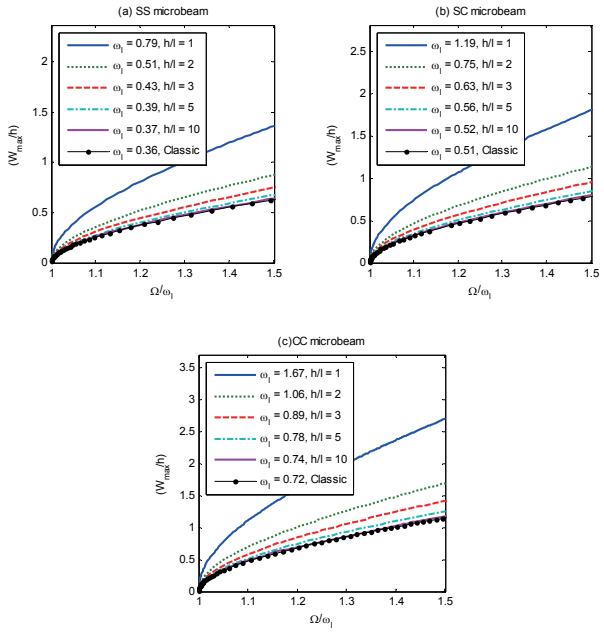


Fig. 3 Maximum of dimensionless transverse deflection versus frequency ratio for different dimensionless length scale parameters based on the MCST ($\eta = 12$, $k = 2$)

against the nonlinear frequency for the first three vibration modes based on the MSGT and classical theory. It is found that the difference between two theories is more significant for higher modes.

6. CONCLUSIONS

In this work, the nonlinear vibration of FG Timoshenko microbeams with different boundary conditions

https://doi.org/10.1017/jmech.2013.65 Published online by Cambridge University Press

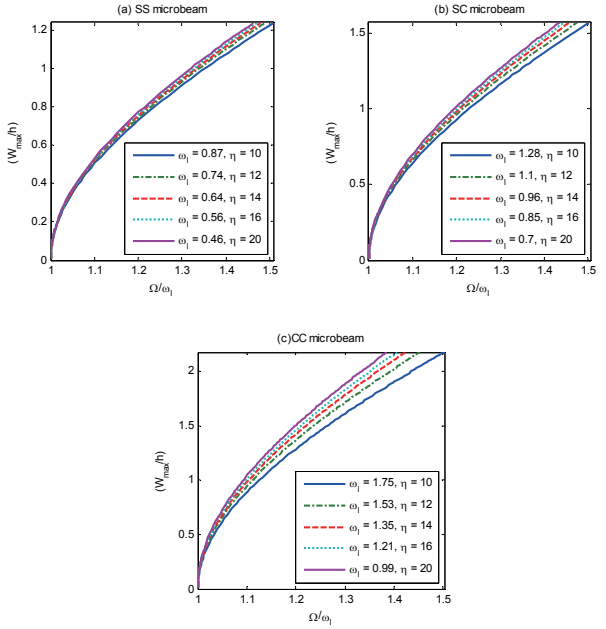


Fig. 4 Maximum of dimensionless transverse deflection versus frequency ratio for different length-to-thickness ratios ($k = 2$, $h/l = 2$)

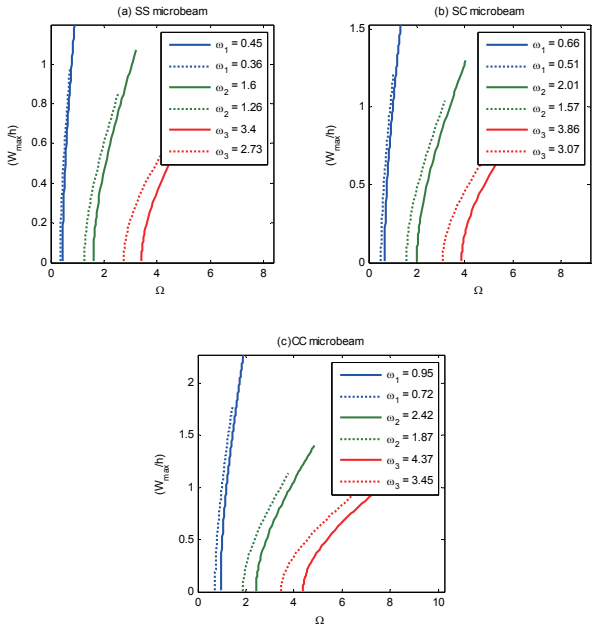


Fig. 5 Maximum of dimensionless transverse deflection versus nonlinear frequency for the first three modes based on the MSGT (solid lines) and classical theory (dashed lines) (η = 12, $k = 2$, $h/l = 5$)

was studied based on the most general form of strain gradient elasticity. In order to derive the governing equations and end conditions, Hamilton's principle was used. The GDQ differential operators were applied to discretize the problem. Then, a numerical Galerkin method was employed to derive the Duffing-type set of equations. The time-domain solution was accomplished based on the HBM together with the Newton-Raphson method. The effects of boundary conditions, length scale parameter, material gradient index, and length-to-thickness ratio on the nonlinear vibration behavior were studied. It was observed that the vibration amplitude and linear frequency decrease with increasing the material gradient index and dimensionless length scale parameter. Also, the significance of the small length scale was shown to be affected by the type of boundary conditions and vibration mode. It was found that the frequencies calculated based on the MSGT are larger than those obtained by the MCST. In addition, the difference between the results obtained by the size-dependent theories and those predicted by the classical theory is significant for small dimensionless length scale parameters and the difference diminishes with increasing the dimensionless length scale parameter.

APPENDIX A

Hadamard and SJT Products:

Definition 1: Let $\mathbf{A}[A_{ij}]_{N\times M}$ and $\mathbf{B}[B_{ij}]_{N\times M}$, then the Hadamard product of these matrices take the form as $\mathbf{A}\circ\mathbf{B}$ $[A_{ij}\,B_{ij}]_{N\times M}$.

Definition 2: Let $\mathbf{A}[A_{ij}]_{N\times M}$ and vector $\mathbf{U} = \{U_i\}_{N\times 1}$, then $\mathbf{A}\,\Diamond\,\mathbf{U}$ $[A_{ij}\,U_i]_{N\times M}$ indicates the postmultiplying SJT product of matrix **A** and vector **U.**

Definition 3: Let $[A_{ij}]_{N\times M}$, and vector $\mathbf{V} = \{v_i\}_{1\times M}$, then $\mathbf{V}^{\mathrm{T}}\,\Diamond\,\mathbf{A}$ $=$ $[A_{ij}\,V_j]_{N\times M}$ indicates the premultiplying SJT product of matrix **A** and vector **V**.

Weighting coefficients of the first and higher-order derivatives:

the weighting coefficients of the first and higher-order derivatives can be evaluated by the following formula

$$\left[\mathbf{D}_{\xi}^{(r)}\right]_{ij} = \mathcal{W}_{ij}^{(r)} = \begin{cases} \mathbf{I}_x\,, & r = 0 \\ \dfrac{\mathcal{P}(\xi_i)}{(\xi_i-\xi_j)\mathcal{P}(\xi_j)}\,, & i\neq j \text{ and } i\,,\ j=1,\ldots,N \text{ and } r=1 \\ r\left[\mathcal{W}_{ij}^{(1)}\mathcal{W}_{ii}^{(r-1)} - \dfrac{\mathcal{W}_{ij}^{(r-1)}}{\xi_i-\xi_j}\right]\,, & i\neq j \text{ and } i\,,\ j=1,\ldots,\ N \text{ and } r=2,3,\ldots N-1 \\ -\sum\limits_{j=1;j\neq i}^{N}\mathcal{W}_{ij}^{(r)}\,, & i=j \text{ and } i\,,\ j=1\,,\ \ldots\,,N \text{ and } r=1,2\,,3\,,\ldots N-1 \end{cases}$$

https://doi.org/10.1017/jmech.2013.65 Published online by Cambridge University Press

where $\mathbf{I}_x$ is a $N \times N$ identity matrix and $\mathcal{P}(x_i) = \prod_{j=1;\mathfrak{J}\neq i}^{N} (\xi_i - \xi_j)$.

APPENDIX B

Integral Operators:

The trapezoidal rule can be used as an integral matrix operator as

$$\int_a^b f(x)\,dx \approx \frac{1}{2}\mathbf{XWF} = \mathbf{S}_x\,\mathbf{F},$$
$$\mathbf{X} = \{x_1, x_2, \ldots, x_N\},$$
$$\mathbf{S}_x = \{S_x\}_{1\times N}$$

where $\mathbf{S}_x$ denotes the integral operator and $\mathbf{W}$ is an $N \times N$ matrix with the non-zero elements of

$$W_{i,j} = \begin{cases} 1, i-j=1 \text{ or } i=j=N \\ -1, i-j=-1 \text{ or } i=j=1 \end{cases}$$

APPENDIX C

$\mathbf{C}_i$ $(i = 1, 2, .., 5)$ appeared in Eq. (35):

$$\mathbf{C}_1 = a_{11}\frac{1}{\eta}(\mathbf{D}_\xi^{(1)}\mathbf{\Phi}_\mathbf{w})\circ(\mathbf{D}_\xi^{(2)}\mathbf{\Phi}_\mathbf{w}) - \frac{a_{33}}{\eta^2}\left(\frac{1}{\eta}(\mathbf{D}_\xi^{(1)}\mathbf{\Phi}_\mathbf{w})\circ(\mathbf{D}_\xi^{(4)}\mathbf{\Phi}_\mathbf{w}) + \frac{3}{\eta}(\mathbf{D}_\xi^{(2)}\mathbf{\Phi}_\mathbf{w})\circ(\mathbf{D}_\xi^{(3)}\mathbf{\Phi}_\mathbf{w})\right)$$

$$\mathbf{C}_2 = \frac{a_{11}}{\eta}\left((\mathbf{D}_\xi^{(1)}\mathbf{\Phi}_\mathbf{u})\circ(\mathbf{D}_\xi^{(2)}\mathbf{\Phi}_\mathbf{w}) + (\mathbf{D}_\xi^{(2)}\mathbf{\Phi}_\mathbf{u})\circ(\mathbf{D}_\xi^{(1)}\mathbf{\Phi}_\mathbf{w})\right) - \frac{a_{33}}{\eta^3}\left((\mathbf{D}_\xi^{(4)}\mathbf{\Phi}_\mathbf{u})\circ(\mathbf{D}_\xi^{(1)}\mathbf{\Phi}_\mathbf{w}) + (\mathbf{D}_\xi^{(3)}\mathbf{\Phi}_\mathbf{u})\circ(\mathbf{D}_\xi^{(2)}\mathbf{\Phi}_\mathbf{w})\right),$$

$$\mathbf{C}_3 = -\frac{b_{11}}{\eta}\left((\mathbf{D}_\xi^{(1)}\mathbf{\Phi}_\psi)\circ(\mathbf{D}_\xi^{(2)}\mathbf{\Phi}_\mathbf{w}) + (\mathbf{D}_\xi^{(1)}\mathbf{\Phi}_\mathbf{w})\circ(\mathbf{D}_\xi^{(2)}\mathbf{\Phi}_\psi)\right) + \frac{b_{33}}{\eta^3}\left((\mathbf{D}_\xi^{(1)}\mathbf{\Phi}_\mathbf{w})\circ(\mathbf{D}_\xi^{(4)}\mathbf{\Phi}_\psi) + (\mathbf{D}_\xi^{(2)}\mathbf{\Phi}_\mathbf{w})\circ(\mathbf{D}_\xi^{(3)}\mathbf{\Phi}_\psi)\right),$$

$$\mathbf{C}_4 = \frac{3a_{11}}{2\eta^2}(\mathbf{D}_\xi^{(2)}\mathbf{\Phi}_\mathbf{w})\circ(\mathbf{D}_\xi^{(1)}\mathbf{\Phi}_\mathbf{w})\circ(\mathbf{D}_\xi^{(1)}\mathbf{\Phi}_\mathbf{w}) - \frac{a_{33}}{\eta^4}\Big(4(\mathbf{D}_\xi^{(1)}\mathbf{\Phi}_\mathbf{w})\circ(\mathbf{D}_\xi^{(2)}\mathbf{\Phi}_\mathbf{w})\circ(\mathbf{D}_\xi^{(3)}\mathbf{\Phi}_\mathbf{w}) + (\mathbf{D}_\xi^{(4)}\mathbf{\Phi}_\mathbf{w})\circ(\mathbf{D}_\xi^{(1)}\mathbf{\Phi}_\mathbf{w})\circ(\mathbf{D}_\xi^{(1)}\mathbf{\Phi}_\mathbf{w}) + (\mathbf{D}_\xi^{(2)}\mathbf{\Phi}_\mathbf{w})\circ(\mathbf{D}_\xi^{(2)}\mathbf{\Phi}_\mathbf{w})\circ(\mathbf{D}_\xi^{(2)}\mathbf{\Phi}_\mathbf{w})\Big),$$

$$\mathbf{C}_5 = -b_{11}\frac{1}{\eta}(\mathbf{D}_\xi^{(1)}\mathbf{\Phi}_\mathbf{w})\circ(\mathbf{D}_\xi^{(2)}\mathbf{\Phi}_\mathbf{w}) + \frac{b_{33}}{\eta^2}\left(\frac{1}{\eta}(\mathbf{D}_\xi^{(1)}\mathbf{\Phi}_\mathbf{w})\circ(\mathbf{D}_\xi^{(4)}\mathbf{\Phi}_\mathbf{w}) + \frac{3}{\eta}(\mathbf{D}_\xi^{(2)}\mathbf{\Phi}_\mathbf{w})\circ(\mathbf{D}_\xi^{(3)}\mathbf{\Phi}_\mathbf{w})\right).$$

REFERENCES

1. Zhang, C., Xu, G. and Jiang, Q., "Analysis of the Air-damping Effect on a Micromachined Beam Resonator," *Mathematics and Mechanics of Solids*, **8**, pp. 315–325 (2003).
2. Elata, D. and Abu-Salih, S., "Analysis of Electromechanical Buckling of a Prestressed Microbeam that is Bonded to an Elastic Foundation," *Journal of Mechanics of Materials and Structures*, **1**, pp. 911–923 (2006).
3. Ramezani, A., Alasty, A. and Akbari, J., "Effects of Rotary Inertia and Shear Deformation on Nonlinear Free Vibration of Microbeams," *Journal of Vibration and Acoustics*, ASME, **128**, p. 611 (2006).
4. Onur Ekici, H. and Boyaci, H., "Effects of Non-Ideal Boundary Conditions on Vibrations of Microbeams," *Journal of Vibration and Control*, **13**, pp. 1369–1378 (2007).
5. Moghimi Zand, M., Ahmadian, M. T. and Rashidian, B., "Semi-Analytic Solutions to Nonlinear Vibrations of Microbeams under Suddenly Applied Voltages," *Journal of Sound and Vibration*, **325**, pp. 382–396 (2009).
6. Fu, Y. and Zhang, J., "Electromechanical Dynamic Buckling Phenomenon in Symmetric Electric Fields Actuated Microbeams Considering Material Damping," *Acta Mechanica*, **215**, pp. 29–42 (2009).
7. Chen, X., Ma, L., Zheng, Y. and Lee, D. W., "Theoretical Analysis of Postbuckling Behavior with Experimental Validation Using Electrothermal Microbeams," *Applied Physics Letters*, **98**, p. 073107 (2011).
8. Krylov, S., R. Ilic, B. and Lulinsky, S., "Bistability of Curved Microbeams Actuated by Fringing Electrostatic Fields," *Nonlinear Dynamics*, **66**, pp. 403–426 (2011).
9. Feng, C., Jiang, L. and Lau, W. M., "Dynamic Characteristics of a Dielectric Elastomer-Based Microbeam Resonator with Small Vibration Amplitude," *Journal of Micromechanics and Microengineering*, **21**, p. 095002 (2011).
10. Chen, X., Ma, L., Zheng, Y., Li, X. and Lee, D. W., "The Influences of Transverse Loads on Electrothermal Post-Buckling Microbeams," *Journal of Micromechanics and Microengineering*, **22**, p. 015011 (2012).
11. Liu, C.-C., Yang, S.-C. and Chen, C.-K., "Nonlinear Dynamic Analysis of Micro Cantilever Beam Under Electrostatic Loading," *Journal of Mechanics*, **28**, pp. 63–70 (2012).
12. Wu, Z., Ma, X., Brett, P. N. and Xu, J., "Vibration Analysis of Submerged Rectangular Microplates with Distributed Mass Loading," *Proceedings of the Royal Society A — Mathematical Physical and engineering Sciences*, **465**, pp. 1323–1336 (2009).
13. Talebian, S., Rezazadeh, G., Fathalilou, M. and Toosi, B., "Effect of Temperature on Pull-In Voltage and Natural Frequency of an Electrostatically Actu-

https://doi.org/10.1017/jmech.2013.65 Published online by Cambridge University Press

ated Microplate," *Mechatronics*, **20**, pp. 666–673 (2010).
14. Xu, L. and Sun, L., "Electromechanical Coupled Non-Linear Vibration of the Microplate," *Proceedings of the Institution of Mechanical Engineers Part C — Journal of Mechanical Engineering Science*, **224**, pp. 1383–1396 (2010).
15. Xu, L. and Sun, L., "Multi-Field Coupled Dynamics for Micro Plate," *International Journal of Applied Electromagnetics and Mechanics*, **35**, pp. 201–229 (2011).
16. Salajeghe, S., Khadem, S. E. and Rasekh, M., "Nonlinear Analysis of Thermoelastic Damping in Axisymmetric Vibration of Micro Circular Thin-Plate Resonators," *Applied Mathematical Modelling*, **36**, pp. 5991–6000 (2012).
17. Fleck, N. A., Muller, G. M., Ashby, M. F. and Hutchinson, J. W., "Strain Gradient Plasticity: Theory and Experiment," *Acta Metallurgica Et Materialia*, **42**, pp. 475–487 (1994).
18. Stölken, J. S. and Evans, A. G., "A Microbend Test Method for Measuring the Plasticity Length Scale," *Acta Materialia*, **46**, pp. 5109–5115 (1998).
19. McFarland, A. W. and Colton, J. S., "Role of Material Microstructure in Plate Stiffness with Relevance to Microcantilever Sensors," *Journal of Micromechanics and Microengineering*, **15**, pp. 1060–1067 (2005).
20. Mindlin, R. D., "Micro-Structure in Linear Elasticity," *Archive for Rational Mechanics and Analysis*, **6**, pp. 51–78 (1964).
21. Mindlin, R. D., "Second Gradient of Strain and Surface Tension in Linear Elasticity," *International Journal of Solids and Structures*, **1**, pp. 417–438 (1965).
22. Mindlin, R. D. and Tiersten, H. F., "Effects of Couple-Stresses in Linear Elasticity," *Archive for Rational Mechanics and Analysis*, **11**, pp. 415–448 (1962).
23. Koiter, W. T., "Couple Stresses in the Theory of Elasticity," *Proceedings of the Koninklijke Nederlandse Akademie van Wetenschappen (B)*, **67**, pp. 17–44 (1964).
24. Yang, F., Chong, A. C. M., Lam, D. C. C. and Tong, P., "Couple Stress Based Strain Gradient Theory for Elasticity," *International Journal of Solids and Structures*, **39**, pp. 2731–2743 (2002).
25. Lam, D. C. C., Yang, F., Chong, A. C. M., Wang, J. and Tong, P., "Experiments and Theory in Strain Gradient Elasticity," *Journal of the Mechanics and Physics of Solids*, **51**, pp. 1477–1508 (2003).
26. Asghari, M., Ahmadian, M. T., Kahrobaiyan, M. H. and Rahaeifard, M., "On the Size-Dependent Behavior of Functionally Graded Micro-Beams," *Materials and Design*, **31**, pp. 2324–2329 (2010).
27. Ke, L. L., Wang, Y. S. and Wang, Z. D., "Thermal Effect on Free Vibration and Buckling of Size-Dependent Microbeams," *Physica E*, **43**, pp. 1387–1393 (2011).
28. Ke, L. L. and Wang, Y. S., "Size Effect on Dynamic Stability of Functionally Graded Microbeams Based on a Modified Couple Stress Theory," *Composite Structures*, **93**, pp. 342–350 (2011).
29. Ansari, R., Gholami, R. and Sahmani, S., "Free Vibration Analysis of Size-Dependent Functionally Graded Microbeams Based on the Strain Gradient Timoshenko Beam Theory," *Composite Structures*, **94**, pp. 221–228 (2011).
30. Ke, L. L., Yang, J., Kitipornchai, S. and Bradford, M. A., "Bending, Buckling and Vibration of Size-Dependent Functionally Graded Annular Microplates," *Composite Structures*, **94**, pp. 3250–3257 (2012).
31. Ansari, R., Gholami, R. and Sahmani, S., "Study of Small Scale Effects on the Nonlinear Vibration Response of Functionally Graded Timoshenko Microbeams Based on the Strain Gradient Theory," *Journal of Computational and Nonlinear Dynamics*, ASME, **7**, p. 031009 (2012).
32. Ke, L. L., Wang, Y. S., Yang, J. and Kitipornchai, S., "Free Vibration of Size-Dependent Mindlin Microplates Based on the Modified Couple Stress Theory," *Journal of Sound and Vibration*, **331**, pp. 94–106 (2012).
33. Kahrobaiyan, M. H., Asghari, M., Hoore, M. and Ahmadian, M. T., "Nonlinear Size-Dependent Forced Vibrational Behavior of Microbeams Based on a Non-Classical Continuum Theory," *Journal of Vibration and Control*, **18**, pp. 696–711 (2012).
34. Ahmadi, A. R., Farahmand, H. and Arabnejad, S., "Buckling Analysis of Rectangular Flexural Microplates Using Higher Continuity P-Version Finite-Element Method," *International Journal for Multiscale Computational Engineering*, **10**, pp. 249–259 (2012).
35. Rajabi, F. and Ramezani, S., "A Nonlinear Microbeam Model Based on Strain Gradient Elasticity Theory with Surface Energy," *Archive of Applied Mechanics*, **82**, pp. 363–376 (2012).
36. Ansari, R., Gholami, R. and Darabi, M. A., "A Nonlinear Timoshenko Beam Formulation Based on a Strain Gradient Theory," *Journal of Mechanics of Materials and Structures*, **7**, pp. 195–212 (2012).
37. Simsek, M., Kocatürk, T. and Akbas, S. D., "Static Bending of a Functionally Graded Microscale Timoshenko Beam Based on the Modified Couple Stress Theory," *Composite Structures*, **95**, pp. 740–747 (2013).
38. Sahmani, S. and Ansari, R., "On the Free Vibration Response of Functionally Graded Higher-Order Shear Deformable Microplates Based on the Strain Gradient Elasticity Theory," *Composite Structures*, **95**, pp. 430–442 (2013).
39. Nateghi, A. and Salamat-Talab, M., "Thermal Effect on Size Dependent Behavior of Functionally Graded Microbeams Based on Modified Couple Stress Theory," *Composite Structures*, **96**, pp. 97–110 (2013).
40. Salamat-Talab, M., Shahabi, F. and Assadi, A.,

https://doi.org/10.1017/jmech.2013.65 Published online by Cambridge University Press

"Size Dependent Analysis of Functionally Graded Microbeams Using Strain Gradient Elasticity Incorporated with Surface Energy," *Applied Mathematical Modelling*, **37**, pp. 507–526 (2013).
41. Ansari, R., Gholami, R., Mohammadi, V. and Faghih Shojaei, M., "Size-Dependent Pull-In Instability of Hydrostatically and Electrostatically Actuated Circular Microplates," *Journal of Computational and Nonlinear Dynamics*, ASME, **8**, p. 021015 (2013).
42. Wang, G. F. and Feng, X. Q., "Effects of Surface Elasticity and Residual Surface Tension on the Natural Frequency of Microbeams," *Applied Physics Letters*, **90**, p. 231904 (2007).
43. Wang, G. F. and Feng, X. Q., "Timoshenko Beam Model for Buckling and Vibration of Nanowires with Surface Effects," *Journal of Physics D: Applied Physics*, **42**, p. 155411 (2009).
44. Sadeghian, H., Goosen, J. F. L., Bossche, A., Thijsse, B. J. and van Keulen, F., "Effects of Size and Surface on the Elasticity of Silicon Nanoplates: Molecular Dynamics and Semi-Continuum Approaches," *Thin Solid Films*, **520**, pp. 391–399 (2011).
45. Liu, J. L., Mei, Y., Xia, R. and Zhu, W. L., "Large Displacement of a Static Bending Nanowire with Surface Effects," *Physica E*, **44**, pp. 2050–2055 (2012).
46. Narendar, S. and Gopalakrishnan, S., "Study of Terahertz Wave Propagation Properties in Nanoplates with Surface and Small-Scale Effects," *International Journal of Mechanical Sciences*, **64**, pp. 221–231 (2012).
47. Timoshenko, S. P. and Goodier, J. N., *Theory of Elasticity*, 3rd Edition, McGraw-Hill, New York (1970).
48. Shu, C., *Differential Quadrature and Its Application in Engineering*, Springer, London (2000).
49. Peng, Z. K., Lang, Z. Q., Billings, S. A. and Tomlinson, G. R., "Comparison Between Harmonic Balance and Nonlinear Output Frequency Response Function in Nonlinear System Analysis," *Journal of Sound and Vibration*, **311**, pp. 56–73 (2008).

(Manuscript received December 21, 2012,
accepted for publication May 31, 2013.)

https://doi.org/10.1017/jmech.2013.65 Published online by Cambridge University Press